Bioactive Materials 14 (2022) 430–442

Contents lists available at ScienceDirect

Bioactive Materials

journal homepage: www.keaipublishing.com/en/journals/bioactive-materials

Dexamethasone-loaded ROS-responsive poly(thioketal) nanoparticles suppress inflammation and oxidative stress of acute lung injury

Zihe Zhai [a,1], Wei Ouyang [b,1], Yuejun Yao [a], Yuqi Zhang [a], Haolan Zhang [a], Feng Xu [b,**], Changyou Gao [a,c,d,*]

[a] MOE Key Laboratory of Macromolecular Synthesis and Functionalization, Department of Polymer Science and Engineering, Zhejiang University, Hangzhou, 310027, China
[b] Department of Infectious Diseases, The Second Affiliated Hospital, Zhejiang University School of Medicine, Hangzhou, 310009, China
[c] Dr. Li Dak Sum & Yip Yio Chin Center for Stem Cell and Regenerative Medicine, Zhejiang University, Hangzhou, 310058, China
[d] Department of Orthopedics, The Second Affiliated Hospital, Zhejiang University School of Medicine, Hangzhou, 310009, China

ARTICLE INFO

Keywords:
Acute lung injury
Reactive oxygen species
Inflammation
Nanoparticles
RNA-Seq

ABSTRACT

Acute lung injury (ALI) is associated with excessive inflammatory response, leading to acute respiratory distress syndrome (ARDS) without timely treatment. A fewer effective drugs are available currently to treat the ALI/ARDS. Herein, a therapeutic nanoplatform with reactive oxygen species (ROS)-responsiveness was developed for the regulation of inflammation. Dexamethasone acetate (Dex) was encapsulated into poly(thioketal) polymers to form polymeric nanoparticles (NPs) (PTKNPs@Dex). The NPs were composed of poly(1,4-phenyleneacetonedimethylene thioketal) (PPADT) and polythioketal urethane (PTKU), in which the thioketal bonds could be cleaved by the high level of ROS at the ALI site. The PTKNPs@Dex could accumulate in the pulmonary inflammatory sites and release the encapsulated payloads rapidly, leading to the decreased ROS level, less generation of pro-inflammatory cytokines, and reduced lung injury and mortality of mice. RNA sequencing (RNA-seq) analysis showed that the therapeutic efficacy of the NPs was associated with the modulation of many immune and inflammation-linked pathways. These findings provide a newly developed nanoplatform for the efficient treatment of ALI/ARDS.

1. Introduction

Inflammation is the defensive response to internal and external stimuli, which helps in eliminating the damaging agents and repairing the damage [1]. However, uncontrolled and excessive inflammation can injure cells, tissues and organs, resulting in systematic damage to the body [2]. The acute lung injury (ALI) is associated with the uncontrolled inflammatory response of host's immune system, which would develop into acute respiratory distress syndrome (ARDS) without timely treatment. For example, the novel strain of coronavirus SARS-CoV-2 (disease COVID-19) can cause lung inflammation and edema, and further develop to ARDS [3]. Unfortunately, it is still lack of effective therapy for the treatment of ALI because of the poorly drug delivery to lung [4,5].

During the progression of ALI, resident alveolar macrophages are firstly activated to the inflammatory M1-like macrophages that release pro-inflammatory cytokines, which would activate the immune response and recruit the white blood cells (WBCs) such as monocytes and neutrophils to the inflamed tissue from capillary and bone marrow [6,7]. Afterwards, the activated neutrophils further release toxic mediators such as reactive oxygen species (ROS) and myeloperoxidase (MPO) to kill and degrade the pathogens. If the pathogens cannot be cleared in time, neutrophils would continue to release ROS, resulting in an overproduction of ROS in the inflamed lung tissue. The high level of ROS not only induces epithelial injury but also activates inflammatory signaling and intensifies immune response [8]. Therefore, reducing the ROS level is a promising way to alleviate lung inflammation.

Peer review under responsibility of KeAi Communications Co., Ltd.
* Corresponding author. MOE Key Laboratory of Macromolecular Synthesis and Functionalization, Department of Polymer Science and Engineering, Zhejiang University, Hangzhou, 310027, China.
** Corresponding author. Department of Infectious Diseases, The Second Affiliated Hospital, Zhejiang University School of Medicine, Hangzhou, 310009, China.
E-mail addresses: xufeng99@zju.edu.cn (F. Xu), cygao@zju.edu.cn (C. Gao).
[1] Zihe Zhai and Wei Ouyang contributed equally to this work.

https://doi.org/10.1016/j.bioactmat.2022.01.047
Received 2 October 2021; Received in revised form 27 January 2022; Accepted 27 January 2022
Available online 11 February 2022

Nowadays, endogenous stimuli-responsive drug delivery systems (DDS) have attracted much more attention because the drug carriers can release their cargos under the trigger of overexpressed signals in the disease microenvironment [9,10]. Among these DDS, the ROS-responsive materials have been developed to deliver therapeutic agents to inflamed lung tissue in a site-specific manner [11,12]. For example, the nanoparticles (NPs) modified with folic acid were prepared by using a kind of ROS-responsive material 4-(hydroxymethyl)phenylboronic acid pinacol ester-modified α-cyclodextrin (Oxi-αCD). The NPs can target to macrophages and release encapsulated antibiotics at the inflammatory sites in a mouse model of pulmonary *P. aeruginosa* infection [13], but their ROS-scavenging ability is limited and the improvement of survival rate of mice is unsatisfactory. Besides, an amphipathic polymer was formulated into a kind of core-shell structured micelles through self-assembly, which can release the payloads through hydrophobic-to-hydrophilic transition of the cores triggered by ROS. *In vivo* results demonstrate that the micelles have effective therapy in acute and chronic inflammation diseases, including ALI, arthritis, and atherosclerosis [14]. However, the mechanism still remains unknown. Furthermore, results from our lab reveal that the ROS-responsive NPs loaded with FK-506 have good performance in suppressing the lung inflammation caused by PM 2.5 [15]. To achieve better therapeutic efficacy, new strategies should be applied by using novel therapeutic systems with stronger ROS eliminating capacity and inflammatory regulation ability, whose mechanisms *in vivo* are also required to be explored.

In this study, a therapeutic nanoplatform is endowed with ROS responsiveness and inflammatory regulation for more effective treatment of ALI. Dexamethasone acetate (Dex), one of the widely used anti-inflammatory glucocorticoids [16], is encapsulated in the NPs composed of a blend of poly(1,4-phenyleneacetonedimethylene thioketal) (PPADT) and polythioketal urethane (PTKU) to obtain PTKNPs@Dex. The massive thioketal bonds in the polymer main chains endow the NPs with fast ROS-responsive degradation and elimination. The loaded Dex is expected to release in response to the inflammation environment with a high level of ROS at ALI, and thereby together decreasing the oxidation degree, suppressing the inflammation and improving the ALI outcome (Scheme 1). Furthermore, the mechanisms of their therapeutic effects *in vivo* will be investigated by RNA-seq.

2. Materials and methods

2.1. Materials

The following chemicals and materials were used as received: 1,4-benzenedimethanethiol (BDT) (Adamas Reagent Co., Ltd., China), 2,2-

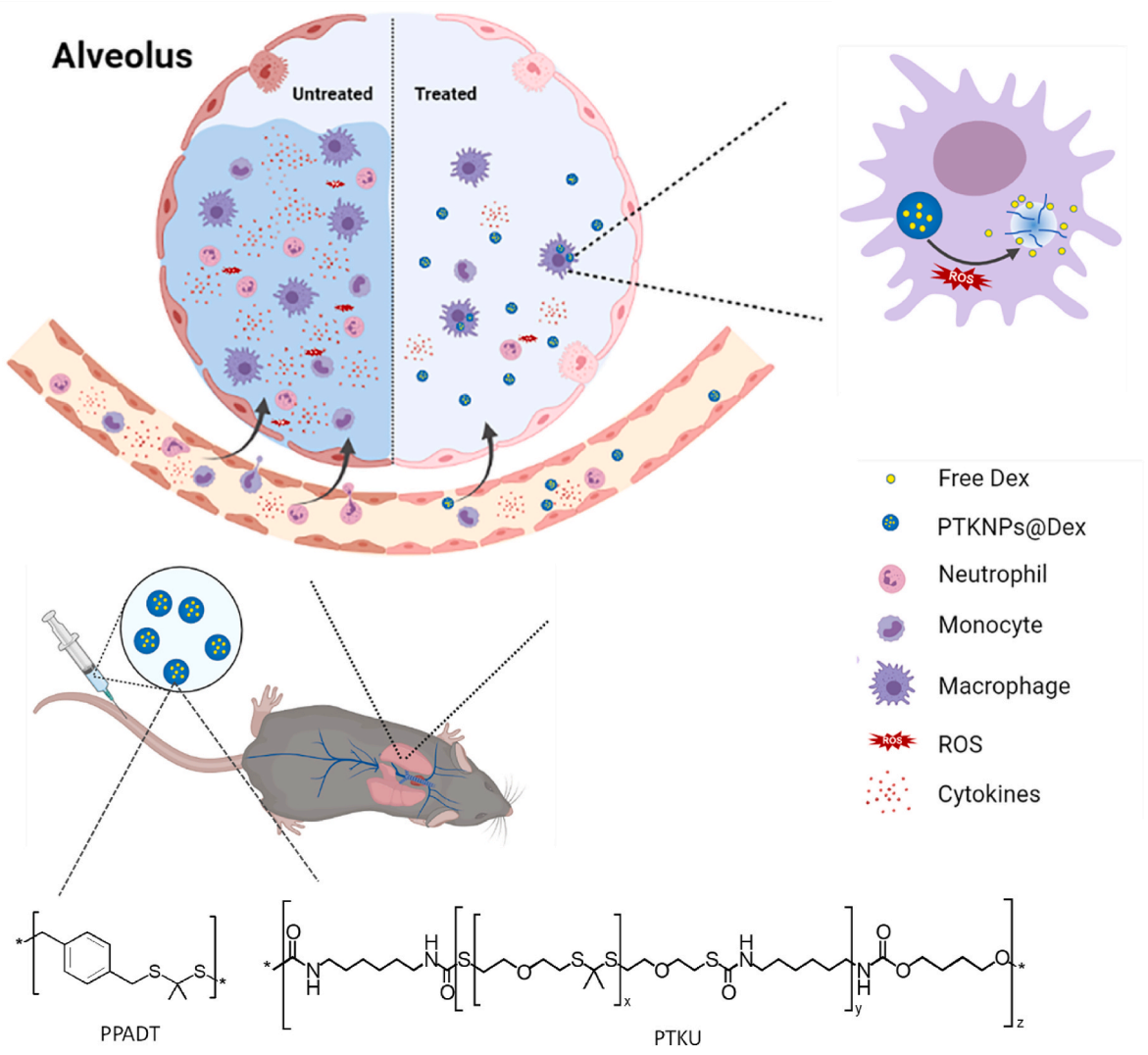

Scheme 1. Scheme to show the *in vivo* therapy of ALI by using ROS-responsive NPs loaded with Dex. The intravenously injected PTKNPs@Dex accumulate in lung, and release drug triggered by the high level of ROS, resulting in decreased immune cell infiltration, a lower level of cytokines and thereby reduced lung injury.

dimethoxypropane (DMP) and Dex (Shanghai Macklin Biochemical Co., Ltd., China), IR 780 (Alfa Aesar), fluorescein (Innochem), 4,6-diamidino-2-phenylindole dihydrochloride (DAPI) (Sigma-Aldrich), Cell Counting Kit-8 (CCK-8) (Topscience Co., Ltd., China); p-toluenesulfonic acid (PTSA) and Nile red (TCI Development Co., Ltd., China); polyvinyl alcohol (PVA) 1788 (alcoholysis degree = 87–89%), bovine serum albumin (BSA) and 1-diphenyl-2-picryl hydrazyl radical (DPPH) (Aladdin Chemistry Co., Ltd., China); dichloromethane (CH_2Cl_2), toluene, acetone, ethyl acetate, toluene, n-hexane, ethanol and dimethyl sulfoxide (DMSO) (Sinopharm Chemical Reagent Company, China); lactate dehydrogenase (LDH) cytotoxicity kit, ROS assay kit, bicinchoninic acid (BCA) protein assay kit, lipid peroxidation malondialdehyde (MDA) assay kit and dihydroethidium (DHE) (Beyotime Biotechnology, China); enzyme-linked immunosorbent assay (ELISA) kit for interleukin-6 (IL-6), tumor necrosis factor-α (TNF-α) (Invitrogen, USA), interleukin-1β (IL-1β) and MPO (Multisciences Biotech, China); Tunel cell apoptosis detection kit and anti-MPO antibody (Servicebio, China). Millipore Milli-Q water with a resistivity of 18.2 MΩ cm^{-1} was used.

2.2. Preparation and characterization of nanoparticles (NPs)

PPADT was synthesized via condensation polymerization [17], which had a molecular weight of 4 kDa and polymer dispersity index (PDI) of 2.17 determined by gel permeation chromatography (GPC). PTKU synthesized in our lab [18] had a molecular weight of 23.8 kDa and PDI of 1.63.

The NPs were prepared via an oil-in-water (O/W) emulsion-solvent evaporation method with slight modification [19]. Briefly, PPADT (7.5 mg) and PTKU (2.5 mg) were dissolved in 1 mL CH_2Cl_2, and was added into 5 mL PVA (w/v, 1%) aqueous solution. The mixture was sonicated using a probe sonicator (amplitude 40%, Sonicator 4000, Misonix, USA) equipped with a probe with a tip diameter of 3.2 mm for 2 min under ice bath. The obtained emulsions were magnetically stirred under water bath (41 °C) for 6 h to evaporate the CH_2Cl_2 completely. Finally, after being centrifuged at 1000 g for 3 min to remove the big aggregates of NPs and un-encapsulated drug, the NPs were collected by centrifugation for 12 min at 10,000 g and washed with water for 3 times. The NPs were re-dispersed in water and kept at 4 °C before use. To prepare the Dex-loaded NPs (PTKNPs@Dex), the Dex (4 mg) was dissolved in acetone (80 μL) and mixed with 1 mL polymer solution before the same procedure was applied. To prepare the fluorescent-labeled NPs, Nile red, IR780 or Cy5.5 was dissolved in CH_2Cl_2 (1 mg/mL), and 100 μL Nile red, IR780 or Cy5.5 solution was mixed with 1 mL polymer solution to prepare the labeled NPs following the same procedure. Fluorescein was dissolved in a mixture of acetone and DMSO, and 100 μL fluorescein solution (10 mg/mL) was mixed with 1 mL polymer solution to prepare the corresponding NPs.

The morphology of the NPs was observed by scanning electron microscopy (SEM) and transmission electron microscopy (TEM). The NPs suspension (10 μL) was dripped on a glass slide and dried at room temperature overnight, before the glass sheet was put on a conducting adhesive and sputter coated with gold. The samples were observed by SEM (S-4800, Hitachi) at an acceleration voltage of 3 kV. The NPs suspension (5 μL) was dripped on a carbon-film-coated copper grid and dried at room temperature overnight for the observation by TEM (JEM-1010) at an acceleration voltage of 120 kV.

The size and polydispersity index of NPs was measured by dynamic light scattering (DLS) using a Zetasizer (Nano-ZS, Malvern, UK). The zeta potential of NPs was measured by laser Doppler electrophoresis, using the same instrument. The NPs colloidal stability was determined by measuring the size and zeta potential after the NPs were incubated in water, phosphate buffered saline (PBS) (0.01 M, pH 7.4) and Dulbecco's modified Eagle medium (DMEM) containing 10% (v/v) fetal bovine serum (FBS) for 24 h at 37 °C.

The drug loading efficiency was acquired by measuring the Dex content of drug-loaded NPs (PTKNPs@Dex) by reversed phase high performance liquid chromatography (HPLC). Firstly, the PTKNPs@Dex suspension (100 μL, containing 1 mg NPs) was freeze-dried for 12 h. The lyophilizate was then dissolved in 0.5 mL CH_2Cl_2, and the solution was sonicated for 1 min to achieve complete dissolution. Next, acetonitrile (0.5 mL, HPLC grade) was added carefully, and the mixture was placed in fume hood overnight to allow the evaporation of CH_2Cl_2, the dissolution of drug and the precipitation of polymer. Then the mixture was centrifuged for 5 min at 2000 g to eliminate the precipitates. The supernatant containing drug was collected, and 20 μL was injected into a HPLC system (Agilent 1100, USA). The detection conditions were set as follows: column (Diamonsil C18, 250 × 4.6 mm, 5 μm), mobile phase (30% acetonitrile/70% aqueous phosphate solution (0.065%, w/v)), flow rate (1.0 mL/min), column temperature (25 °C), and detection by the absorbance of 234 nm at 9.9 min. The drug concentration in each sample was calculated using a calibration curve created with known concentrations of Dex. The drug loading content (LC) and drug encapsulation efficiency (EE) were calculated according to the weight ratios of the loaded drug to the drug-loaded NPs and to the weight of feeding drug, respectively.

2.3. ROS responsiveness of NPs

2.3.1. ROS-responsive degradation of NPs

The ROS-responsive degradation of NPs was analyzed by monitoring the structure and transmittance change of NPs. The structure change of NPs exposing to ROS was measured by ^{1}H nuclear magnetic resonance (^{1}H NMR). The freeze-dried PTKNPs were incubated in a mixture of DMSO-d_6 and water with 100 mM H_2O_2 or 1 mM ·OH (generated from reaction of H_2O_2 and Fe^{2+}) at 37 °C in a shaker of 100 rpm for 24 h. Then the NPs were freeze-dried for 6 h, and dissolved in $CDCl_3$ for ^{1}H NMR (Bruker DMX500) analysis. The transmittance change of PTKNPs suspension was monitored by a UV–Vis spectrophotometer. The NPs suspension (0.2 mg/mL) was incubated in 0.5 mM ·OH, 1 mM ·OH at 37 °C, respectively. Each sample was prepared in triplicate. The transmittance of each sample was measured at 550 nm by a UV–Vis spectrophotometer (Shimadzu UV-1800, Japan) at each predetermined time interval.

2.3.2. ROS-scavenging ability of NPs

The free radical-scavenging ability of NPs was measured by using DPPH with slight modification [20]. Briefly, the DPPH ethanol solution (at a final concentration of 0.2 mM) was mixed with the NPs suspension with final concentrations of 100, 250, 500, 750, 1000 μg/mL, respectively. The mixture was placed in a shaker of 100 rpm at 37 °C for 30 min, and then centrifuged at 10,000 g for 12 min. The absorbance of supernatant of each sample was measured by a microplate reader (Infinite M200 Pro, Tecan) at 517 nm. Each sample was prepared in triplicate.

2.3.3. ROS-responsive drug release of NPs

Nile red as a model drug was encapsulated into the NPs to simulate the drug release behavior of NPs. The Nile red-loaded NPs suspension (0.1 mg/mL) was incubated with 0.5 mM ·OH, 1 mM ·OH, 100 mM H_2O_2 and 500 mM H_2O_2 at 37 °C, respectively. Each sample was prepared in triplicate. At each predetermined time interval, 150 μL NPs suspension was collected and placed in a 96 flat bottom black polystyrene plate. The emission fluorescence (F.L.) intensity at 607 nm was measured with an excitation wavelength of 550 nm by a microplate reader. The accumulative Nile red release was calculated according to the following formula:

$$\textit{Accumulative Nile red release}\ (\%) = \frac{F.L.\ intensity(t_0) - F.L.\ intensity(t)}{F.L.\ intensity(t_0)} \times 100\%$$

Where t_0 and t refer to the time at start and each predetermined time interval, respectively.

2.4. Cell culture in vitro

Murine macrophage cell line RAW264.7 was obtained from the Cell Bank of Typical Culture Collection of the Chinese Academy of Sciences (Shanghai, China). The RAW264.7 cells were cultured in high-glucose DMEM (Gibco, USA) containing 10% FBS (Gibco, USA), 100 U/mL penicillin and 100 μg/mL streptomycin. The FBS was inactivated by heating at 56 °C for 30 min before use. The cells were incubated in an incubator at 37 °C supplied with 5% CO_2 and 100% humidity.

2.4.1. Cytotoxicity of NPs

The cytotoxicity of NPs was determined by CCK-8 and LDH assay. RAW264.7 cells were seeded at a density of 1×10^4 per well on the 96-well plates. After 12 h, the medium was replaced with a medium containing different concentrations of NPs. After 24 h of incubation, the NPs were removed by washing 3 times with PBS. For CCK-8 assay, the cells were incubated with a medium containing 10% (v/v) CCK-8 for another 3 h, then the absorbance at 450 nm was measured by a microplate reader. For LDH assay, the cells were incubated with LDH releasing reagent for another 1 h, followed by the addition of LDH detecting reagent. After 30 min, the absorbance at 490 nm was measured by a microplate reader. Besides, after the RAW264.7 cells were stimulated by lipopolysaccharide (LPS) (1 μg/mL), the cytotoxicity of PTKNPs (5 μg/mL), free Dex (0.3 μg/mL) and PTKNPs@Dex (5 μg/mL) after incubation with cells for 24 h was also checked by CCK-8 assay.

2.4.2. Cellular uptake

The cellular uptake of the NPs was analyzed by flow cytometry and confocal laser scanning microscopy (CLSM). For the CLSM assay, the RAW264.7 cells were seeded at a density of 20×10^4 on the laser confocal cell culture dish (35 mm). After 24 h, the cells were incubated with a medium containing LPS (1 μg/mL) for 1 h. Subsequently, the fluorescein-loaded NPs were added at a final concentration of 20 μg/mL, and the cells were further incubated for 2, 4 and 6 h, respectively. After the free NPs were removed by washing with PBS for 3 times, the cells were fixed with 4% paraformaldehyde (PFA) at 4 °C overnight. The cells were washed with PBS for 3 times, and were then permeabilized with 0.5% (v/v) Triton X-100/PBS solution at 37 °C for 5 min, followed by washing with PBS for 3 times. BSA/PBS solution (1%, w/v) was added, and incubated with the cells for 1 h at room temperature, followed by washing with PBS. Then, DAPI/PBS solution (2 μg/mL) was added and incubated at 37 °C for another 1 h in the dark. Finally, the cells were washed with PBS for 3 times, and observed under CLSM (Leica TCS SP5, Germany).

For the flow cytometry assay, the RAW264.7 cells were seeded at a density of 8×10^4 per well on the 24-well plates. After 12 h, the cells were incubated with a medium containing LPS (1 μg/mL) for 1 h. Subsequently, the fluorescein-loaded NPs were added at a final concentration of 20 μg/mL, and the cells were further incubated for 2, 4 and 6 h, respectively. After the free NPs were removed by washing with PBS for 3 times, the cells were collected and centrifuged at 500 g for 5 min. Then the cells were re-dispersed in PBS, and the average F.L. intensity per cell and the ratio of cells with fluorescence was measured with flow cytometry (FACS Calibur, BD).

2.4.3. Intracellular ROS level inhibition of NPs

The intracellular ROS levels were measured using a ROS assay kit. The RAW264.7 cells were plated in 12-well plates (1×10^5 cells per well) overnight, and then pretreated with free Dex (0.3 μg/mL), PTKNPs (5 μg/mL) or PTKNPs@Dex (5 μg/mL) for 2 h. Next, the cells were stimulated with 1 μg/mL LPS for another 4 h. Finally, the cells were incubated with 2,7-dichlorodihydrofluorescein diacetate (DCFH-DA) (10 μM) for 30 min at 37 °C, and observed under a fluorescence microscope (Leica DMi8).

2.4.4. Inflammatory cytokines protein and mRNA expression analysis in vitro

The RAW264.7 cells were plated in 12-well plates (1×10^5 cells per well) overnight. Then the cells were stimulated with 1 μg/mL LPS for 12 h after pretreatment with free Dex, PTKNPs or PTKNPs@Dex for 2 h. The cytokines including IL-6, TNF-α and IL-1β in the supernatant were measured using ELISA kits according to the manufacturer's instructions. Total RNA was isolated from RAW264.7 cells using an Ultrapure RNA kit (Cwbiotech, China) according to the manufacturer's protocol. Equal amount of total RNA (1 μg) was reverse-transcribed to cDNA using PrimeScript™RT reagent Kit with gDNA Eraser (Takara, Japan). Then the cDNA products were subjected to quantitative PCR (qPCR) analysis with SYBR Premix Ex Taq™ and carried on Applied Biosystems 7500. The primer sequences for target genes are listed in Table S1. The housekeeping gene β-actin was utilized to normalize the fold induction of transcript based on the $2^{-\Delta\Delta}$Ct method.

2.5. Animal experiments

All animal experiments were approved by Animal Care and Use Committee of the Second Affiliated hospital of Zhejiang University (Hangzhou, China). Pathogen free, female C57BL/6 mice (6–8 weeks old) were obtained from the Animal Center of Slaccas (Shanghai, China).

2.5.1. Animal model establishment and treatment

To establish the mouse ALI model, the C57BL/6 mice were intratracheally (*i.t.*) injected with LPS as described previously [21]. Two hours after LPS (5 mg/kg) administration, the mice were intravenously (*i.v.*) injected with 150 μL PBS, PTKNPs (suspensions in PBS, 8.67 mg/mL), free Dex (dissolved in DMSO, 4 mg/kg), or PTKNPs@Dex (suspensions in PBS, 8.67 mg/mL, equal to 4 mg/kg of free Dex), respectively. The mice treated with only PBS were used as controls. Then the mice were sacrificed at 24 h after LPS treatment to collect the bronchoalveolar lavage fluid (BALF) and lung tissues. For mortality, the mice were intratracheally challenged with LPS (50 mg/kg), and administered with the same amount of formulations as described above. The survival rate was monitored every 24 h until 7 d.

2.5.2. NPs distribution in vivo

The mice were injected intravenously with IR 780-labeled NPs (150 μL, 8.67 mg/mL) 2 h after ALI model was created. Control mice were intravenously injected with PBS. At 4, 8, 24, 48, 72 and 96 h after NPs administration, the mice were euthanized, and the major organs including heart, liver, spleen, lung and kidney were collected and imaged *ex vivo* by IVIS Spectrum Imaging System (CLS136341/F, PerkinElmer). The average fluorescence intensity was processed by the Living Imaging software (Living Image ®, PerkinElmer, USA).

2.5.3. Wet/dry ratios of lung

The mice were sacrificed 24 h after LPS challenge. After dissection, the right lung was collected for obtaining the "wet" weight. Then it was placed in an oven at 65 °C for 72 h to obtain the "dry" weight. Lung edema was measured by calculating the lung wet/dry (W/D) ratio.

2.5.4. Lung histology and immunohistochemistry

The lungs, hearts, livers, spleens, and kidneys of mice were fixed and immersed in 4% PFA overnight. Tissue sections were cut into serial 5 μm thickness and stained with hematoxylin and eosin (H&E). Images of the stained sections were collected with the Pannoramic Midi II histoscanner (3DHISTECH, Hungary). Lung injury was assessed blindly according to the four categories: interstitial inflammation, neutrophil infiltration, congestion and edema. The severity of lung injury was graded on a 0 to 4 scale: 0 = no injury; 1 = up to 25% injury of the field; 2 = up to 50% injury of the field; 3 = up to 75% injury of the field; and 4

= diffused injury. The score of each mouse was calculated as the mean of four lung sections [22].

For MPO assay, the lung tissues were fixed in 4% PFA, embedded in paraffin and cut into 5 μm thick sections. The tissue slices were blocked with 0.5% BSA for 1 h and incubated overnight at 4 °C with anti-MPO antibody. Then a secondary anti-mouse IgG antibody were incubated for 1 h at 37 °C. Images of the stained sections were collected with the Pannoramic Midi II histoscanner. The relative MPO expression was analyzed by Image J software. For Tunel assay, the paraffin sections of lungs were placed on glass slides. After repair with proteinase K, the samples were permeabilized and incubated with Tunel reaction solution. Then DAPI was added for nuclei detection. Images were collected with the Pannoramic scanner as mentioned above. The relative fluorescence intensity was analyzed by Image J software.

2.5.5. Lung lipid peroxidation assay

The lung tissues were weighed and homogenized in ice-cold lysis buffer containing 1 mM phenylmethylsulfonyl fluoride and protease inhibitor cocktail (Beyotime Biotechnology, China). Then, the homogenates were centrifuged at 12,000 g for 15 min at 4 °C to collect the supernatant. The MDA level was determined with a lipid peroxidation MDA assay kit according to the manufacturer's instructions.

2.5.6. ROS level in lung tissue

For detection of the ROS level *in vivo*, the fresh lung tissues were embedded in Tissue-Tek OCT and cut into 10 μm thickness with a frozen microtome. Slices were stained with 10 μM DHE and incubated in a light-protected humidified chamber at 37 °C for 30 min to detect ROS production. Nuclei were stained with DAPI solution for 10 min. The samples were observed with Pannoramic Midi II histoscanner (3DHISTECH, Hungary). The relative fluorescence intensity was analyzed by Image J software.

2.5.7. Collection and analysis of BALF

The BALF was collected through the lavage of lungs using a tracheal cannula with 0.8 mL of ice-cold PBS for 3 times. After removing the erythrocytes in the BALF by lysis buffer, the total cell number was counted. Cells (2×10^5) were loaded onto a slide by using a cytospin and stained with Giemsa regent for cell differentiation. BALF protein concentrations were determined using the BCA protein assay kit. LDH concentration in BALF was determined with LDH assay kit (Nanjing Jiancheng Bioengineering Institute). The levels of MPO, IL-6, TNF-α and IL-1β in BALF were measured by ELISA kits according to the manufacturer's instructions.

2.5.8. Dex concentration in lung tissue

To determine the concentration of Dex released by PTKNPs@Dex in lung tissue, the ALI mice were administrated with free Dex and PTKNPs@Dex, respectively. After 4 h, the mice were sacrificed and the lung tissues were collected, weighted, homogenized and freeze-dried. Then Dex was extracted by incubation the treated lung tissues in CH_2Cl_2 and acetonitrile. After centrifugation, the Dex level in the supernatant was determined by HPLC.

2.5.9. Western blotting (WB)

The proteins were extracted from cultured cells or lung tissues using lysis buffer containing 1 mM phenylmethylsulfonyl fluoride and protease inhibitor cocktail. After the measurement of protein concentration by the BCA protein assay kit, a routine Western blot analysis was performed. The samples were separated by SDS-PAGE gel and transferred to poly(vinyl difluoride) (PVDF) membranes. After blocking with 5% non-fat milk, the membranes were incubated with primary antibodies at 4 °C overnight. Then the membranes were treated with horseradish peroxidase-conjugated secondary antibodies and visualized using the chemiluminescence system (GE ImageQuant™ 800).

2.5.10. Flow cytometry

The ALI mice were treated with Cy5.5-labeled NPs for 22 h. The cell suspensions in BALF were stained with anti-CD11b-AF488, anti-CD11c-APC, anti-F4/80-BV421, and anti-Ly6G-BV785 antibodies (BioLegend), and analyzed using CytoFLEX flow cytometer (Beckman Coulter, Inc.). Data were analyzed with FlowJo software X.

2.5.11. The mRNA expression analysis in vivo

The mRNA levels of *Il-6, Tnf-α, Il-1β, Cxcl9, Ccl4, Csf3, Cxcl2, Ccl3 and Nos2* in lung tissue were measured by qPCR analysis as mentioned above. The primer sequences are listed in Table S1.

2.5.12. RNA-seq analysis

The total RNA of lung tissues was extracted using animal tissue RNA purification kit, TRK1002 (LC Science, Houston, TX). The purity, concentration, and integrity of the total RNA samples were assessed prior to further analysis. The purified mRNA was fragmented and reverse-transcribed to create the final cDNA library in accordance with the protocol for the mRNA-Seq sample preparation kit (Illumina, San Diego, USA). The cDNA libraries were then sequenced using the Illumina sequencing technology on an Illumina Hiseq 4000 at LC Bio (Zhejiang, China) according to the manufacturer's instructions. Finally, paired-end reads were produced after removing low quality reads. The clean data were aligned to the UCSC (http://genome.ucsc.edu/) mouse reference genome using HISAT package. StringTie was used to perform the expression level of mRNAs by calculating FPKM. The differentially expressed genes (DEGs) were selected with $|\log2FC| \geq 1.0$ and statistical significance ($p < 0.05$) by Ballgown R package. The volcano plot, heatmap, Venn diagrams, GO and KEGG enrichment analysis of DEGs were generated with OmicStudio tools with clusters Profiler R package (https://www.omicstudio.cn/index). The protein-protein interaction (PPI) network of DEGs was obtained from the STRING database and visualized using Cytoscape software. The top ten hub genes were identified using a plugin of Cytoscape, Cyto-Hubba, based on the maximal clique centrality (MCC) calculation method.

2.5.13. Systemic inflammation and oxidative stress

The blood of mice was collected and stored at room temperature for 2 h. After centrifugation, the serum was obtained. The IL-6, TNF-α and MDA levels in serum were measured by ELISA and MDA assay kits respectively according to the manufacturer's instructions.

2.6. Statistical analysis

All the results were expressed as mean ± standard deviation (SD) unless otherwise stated. Statistical significance among multiple groups was analyzed using the one-way analysis of variance (ANOVA) and between two groups using Student's *t*-test. The survival rate was analyzed using a log-rank test. P values less than 0.05 were considered statistically significant (*$P < 0.05$, **$P < 0.01$, ***$P < 0.001$ and ****$P < 0.0001$).

3. Results and discussion

3.1. Preparation and characterization of NPs

The ROS-responsive polymer PPADT had a relatively low molecular weight (4 kDa) and is thus degraded very fast [17]. Due to the low glass transition temperature (Tg) (Tg = 5 °C), the NPs prepared of PTKU easily undergo aggregation and morphology alteration over time [18]. In this study, PPADT and PTKU (w/w, 3:1) were blended to prepare the NPs with better stability, morphology (Fig. S1) and drug loading and release properties that are mandatory for intravenous administration for ALI therapy, which is convenient but rarely adopted for the nanotherapeutic system.

The blank NPs (PTKNPs) and Dex-loaded NPs (PTKNPs@Dex) were prepared using an O/W emulsion-solvent evaporation method. SEM and

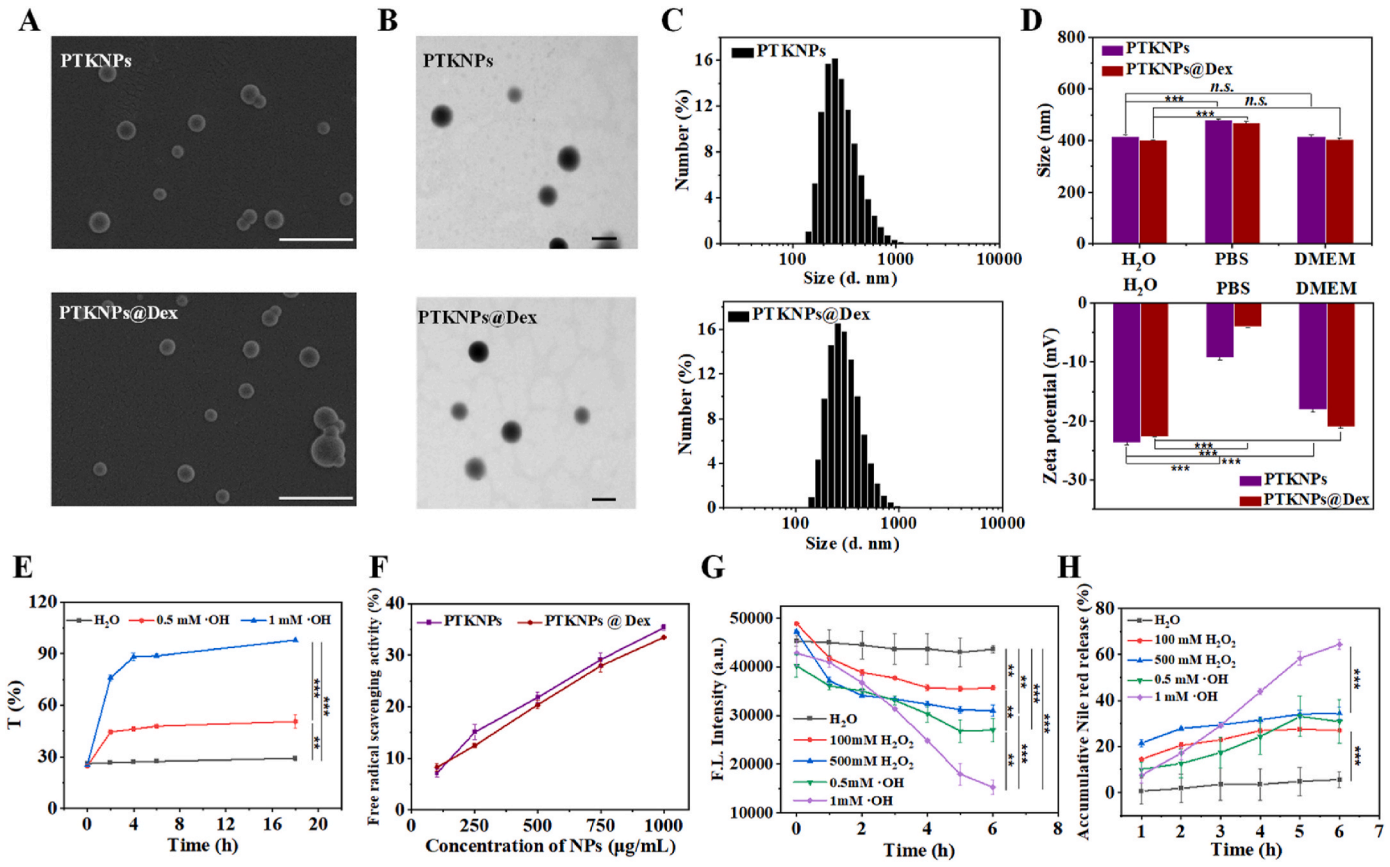

Fig. 1. Characterizations of NPs. (A) SEM and (B) TEM images of PTKNPs and PTKNPs@Dex. Scale bars for SEM and TEM are 1 μm and 200 nm, respectively. (C) Size distribution of PTKNPs and PTKNPs@Dex measured by DLS. (D) Variation of size and zeta potential of PTKNPs and PTKNPs@Dex measured by DLS after being incubated in different mediums at 37 °C for 24 h. (E) Transmittance change of NPs suspension measured by UV–Vis spectroscopy after being incubated in water and different concentrations of ·OH at 37 °C. (F) Free radical-scavenging ability of PTKNPs and PTKNPs@Dex monitored by DPPH assay. (G) F.L. intensity of Nile red-loaded NPs and (H) accumulative Nile red release after being incubated with different concentrations of ·OH and H_2O_2, respectively. *$p < 0.05$, **$p < 0.01$, and ***$p < 0.001$; n.s., no significant difference at $p < 0.05$.

TEM found that both the PTKNPs and PTKNPs@Dex had a spherical morphology (Fig. 1A and B) with an average diameter of 311 nm and 307 nm (Fig. 1C), respectively. The Dex LC and EE were 6% and 9.9% determined by HPLC by referring to the calibration curve (Fig. S2), respectively. After being incubated in different mediums for 24 h, the zeta potential of the NPs in PBS decreased significantly and the size enlarged slightly compared to those in water (Fig. 1D) due to the electrostatic interaction between the cations in PBS and the negative charged groups on the NPs surface. The NPs showed excellent colloidal stability in DMEM containing 10% FBS, and their zeta potential decreased only slightly as a result of protein adsorption on their surface. No aggregation was found, revealing again their good colloidal stability.

To investigate the ROS responsiveness of the NPs, the degradation products of NPs after being exposed to ROS were determined by ^{1}H NMR (Fig. S3). A new peak of the proton resonance signals at 2.08 ppm appeared in the presence of 1 mM ·OH, which is consistent with the generation of acetic acid as a result of reaction between ·OH and thioketal linkage and further oxidation of the intermediate acetone by excess ·OH [23]. Similarly, the incubation with 100 mM H_2O_2 generated acetone, as shown by the new peak of protons at 2.17 ppm. These results reveal that the thioketal-segmented NPs can respond to ROS and are degraded into small molecules. Besides, degradation of the NPs decreased the light scattering, leading to the increase of transmittance of NPs suspension as shown in Fig. S4 and Fig. 1E. The transmittance even reached to nearly 100% and the NPs suspension became totally transparent after being incubated in 1 mM ·OH for about 1 d. The radical-scavenging efficiency increased almost linearly along with the increase of NPs concentration regardless of the Dex loading, as proved by the DPPH scavenging experiment (Fig. 1F) [20]. More than 30% DPPH was eliminated within 30 min when the NPs concentration was 1 mg/mL, revealing that the NPs can respond and eliminate ROS rapidly.

The NPs would react and consume ROS, and meanwhile are degraded to release the encapsulated payloads on demand at inflammatory conditions, creating a typical self-adaptive NPs system for drug delivery. Nile red, a hydrophobic fluorescence dye, was thus used to monitor this process because its fluorescence can be quenched in a water-rich environment [24–26]. The Nile red released from NPs was negligible in water along with time prolongation, demonstrating the NPs are stable and thus the drugs can be well maintained inside the NPs during transportation (Fig. 1G and H). Under the treatment of H_2O_2 and ·OH, the fluorescence intensity of NPs decreased, and higher concentrations of ROS resulted in faster release along with time prolongation, suggesting the sustained release of Nile red and self-adaptive nature of the ROS-responsive NPs system. The release of Nile red became less apparent after 4–5 h in 100 mM H_2O_2, 500 mM H_2O_2 and 0.5 mM ·OH, whereas continually increased in 1 mM ·OH at 6 h, and the released percentage of Nile red reached over 60% in 1 mM ·OH, which was doubled compared with other conditions. These results reveal that the NPs are more sensitive to ·OH than to H_2O_2, the drug release can be triggered by ROS in a controlled but different manner. The reason is that ·OH is a kind of more active and destructive ROS, thus the thioketal bond in the NPs would respond to ·OH more easily with a faster rate.

3.2. Cytotoxicity and cellular uptake of NPs

Macrophages are considered to play a vital effect on the progression of ALI [8]. Macrophages located in alveoli are the first defender to be activated by pathogens, which play a featured role in initiating and maintaining the inflammatory response [27]. Both the LDH release (Fig. S5A) and CCK-8 assay (Fig. S5B) reveal that the PTKNPs and PTKNPs@Dex had no obvious toxicity to RAW264.7 cells within the investigation range of 1–20 μg/mL. After LPS stimulation, the cell viability was increased, which was not influenced by the incubation of PTKNPs (Fig. S5C). Free Dex inhibited the cell viability, but the PTKNPs@Dex not, suggesting that the PTKNPs as a carrier could protect cells from drug toxicity and avoiding exposure of cells to a high concentration of drug. To investigate the cellular uptake of NPs in an inflammatory condition, the RAW264.7 cells were activated by LPS stimulation. Fig. 2A and B show that the NPs were readily internalized at 2 h of co-incubation, and their amount increased over time. At 6 h, over 50% of the RAW264.7 cells had endocytosed the NPs. The internalized NPs were mainly located in cytoplasm and partly around cell nuclei (Fig. 2C). None of the NPs penetrated into nuclei, because their size was

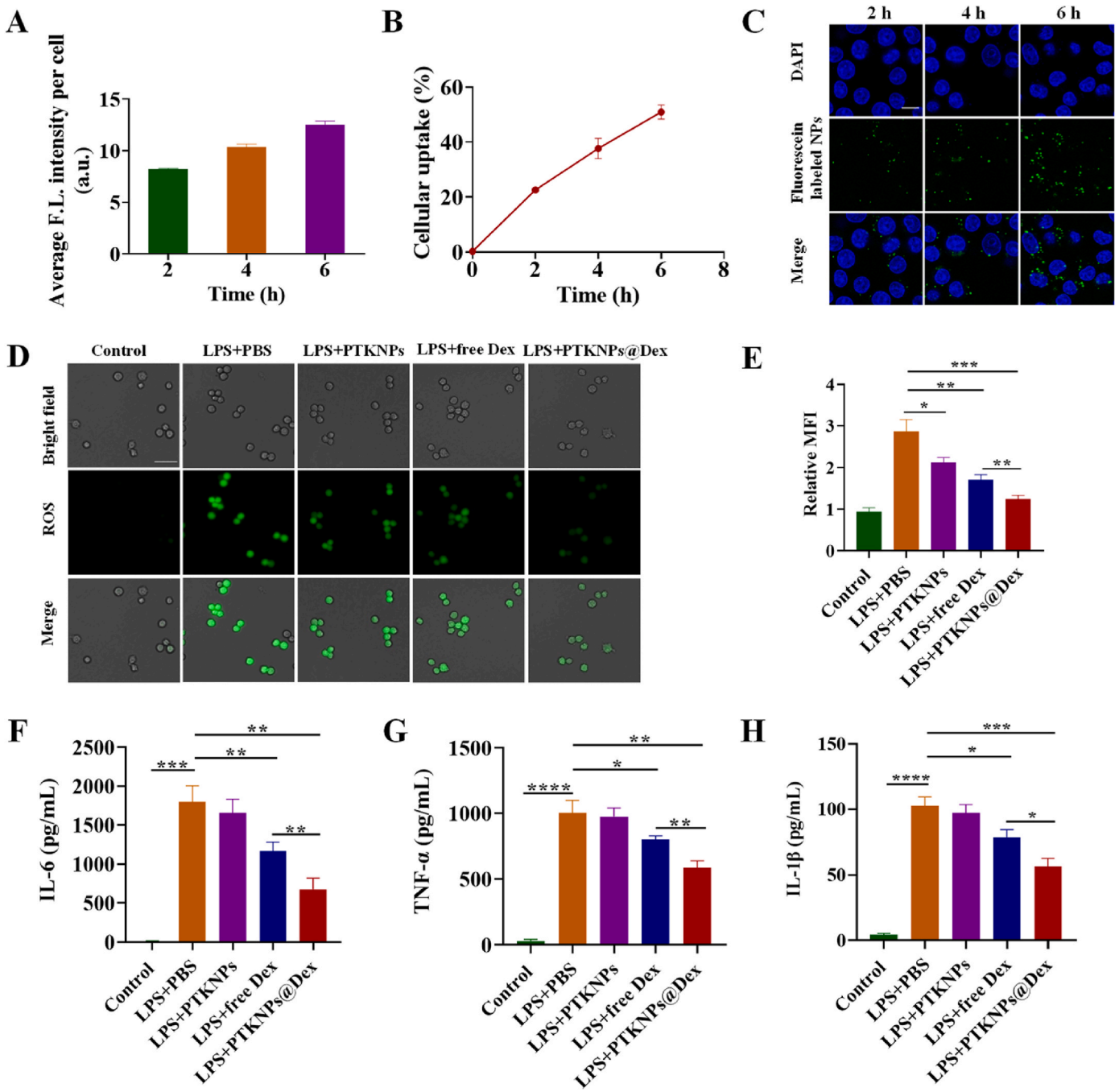

Fig. 2. Cellular uptake and anti-inflammatory effects of NPs *in vitro*. (A) Average F.L. intensity per cell, (B) ratio of cells with fluorescence, and (C) CLSM images at various incubation time. The NPs were labeled with fluorescein (green), and the cell nuclei were stained with DAPI (blue). Scale bar, 10 μm. (D) Representative images and (E) relative mean fluorescence intensity (MFI) of intracellular ROS generation in RAW264.7 cells. ROS were visualized by staining with DCFH-DA (green). Scale bar, 20 μm. (F) IL-6, (G) TNF-α, and (H) IL-1β secreted by RAW264.7 cells after activation by LPS and treatment with PBS, PTKNPs, free Dex, or PTKNPs@Dex. *$p < 0.05$, **$p < 0.01$, ***$p < 0.001$, and ****$p < 0.0001$.

much larger than those of nucleopores (25–30 nm) [28]. These findings suggest that the NPs can be rapidly internalized by activated macrophages, bringing the possibility of drug release inside/around the inflammatory cells and in turn suppression of the inflammation.

3.3. ROS inhibition and anti-inflammation effect of NPs in vitro

The overproduced ROS contribute to injury and amplify inflammation process [29]. As shown in Fig. 2D, ROS were overexpressed after LPS stimulation, with bright green fluorescence in the RAW264.7 cells. The PTKNPs alone decreased the ROS level significantly due to their scavenge ability of free radicals, whereas the free Dex also inhibited significantly the production of ROS because of its intrinsic anti-inflammatory function (Fig. 2E). The PTKNPs@Dex had the strongest ROS-inhibition effect due to their combination effects.

Stimulated by pathogens, the macrophages would polarize to the pro-inflammatory state of M1 phenotype, and thereby secrete pro-inflammatory cytokines such as IL-6, TNF-α and IL-1β, which play an important role in the development and progression of inflammation in ALI [27]. ELISA (Fig. 2F–H) and qPCR (Figs. S6A–C) analyses confirmed that the LPS-stimulated macrophages indeed expressed significantly high levels of IL-6, TNF-α and IL-1β, which could not be suppressed by the PTKNPs alone. Free Dex treatment reduced the cytokine levels to some extent, whereas the PTKNPs@Dex treatment resulted in the lowest levels of these cytokines. These results suggest that the PTKNPs@Dex synergistically suppress the production of key pro-inflammatory cytokines via the interplay of ROS-scavenging polymers and inflammation-suppression Dex and/or the enhanced release of Dex inside cells.

3.4. Distribution and safety evaluation of NPs in vivo

The ROS elimination and inflammation suppression abilities of the PTKNPs@Dex *in vitro* convey their therapeutic role for the ALI therapy *in vivo*. Intravenous (*i.v.*) injection is the most important administration way for drugs in clinical application. Previous studies have shown that large size nanoparticles are more easily accumulated in lung [30,31]. Therefore, it is important to investigate whether the NPs can accumulate in the inflammatory lung tissue after intravenous injection. For this purpose, the IR780-labeled NPs were injected to the ALI mice via tail vein. At different time intervals post injection, the lungs, livers, spleens, hearts and kidneys were collected and imaged by an *ex vivo* fluorescence imaging system. Figs. S7A and B show that stronger fluorescence was recorded in the livers, spleens and lungs within 4 h, whereas very weak signals were detected from the hearts and kidneys. However, the signals in the lungs slightly increased and then decreased along with time prolongation, suggesting that more and more NPs would accumulate in the lungs at first, then the inflammatory microenvironment in ALI can trigger the degradation of NPs and thereby release the dye molecules. It is worth mentioning that the NPs still accumulated in other vital organs

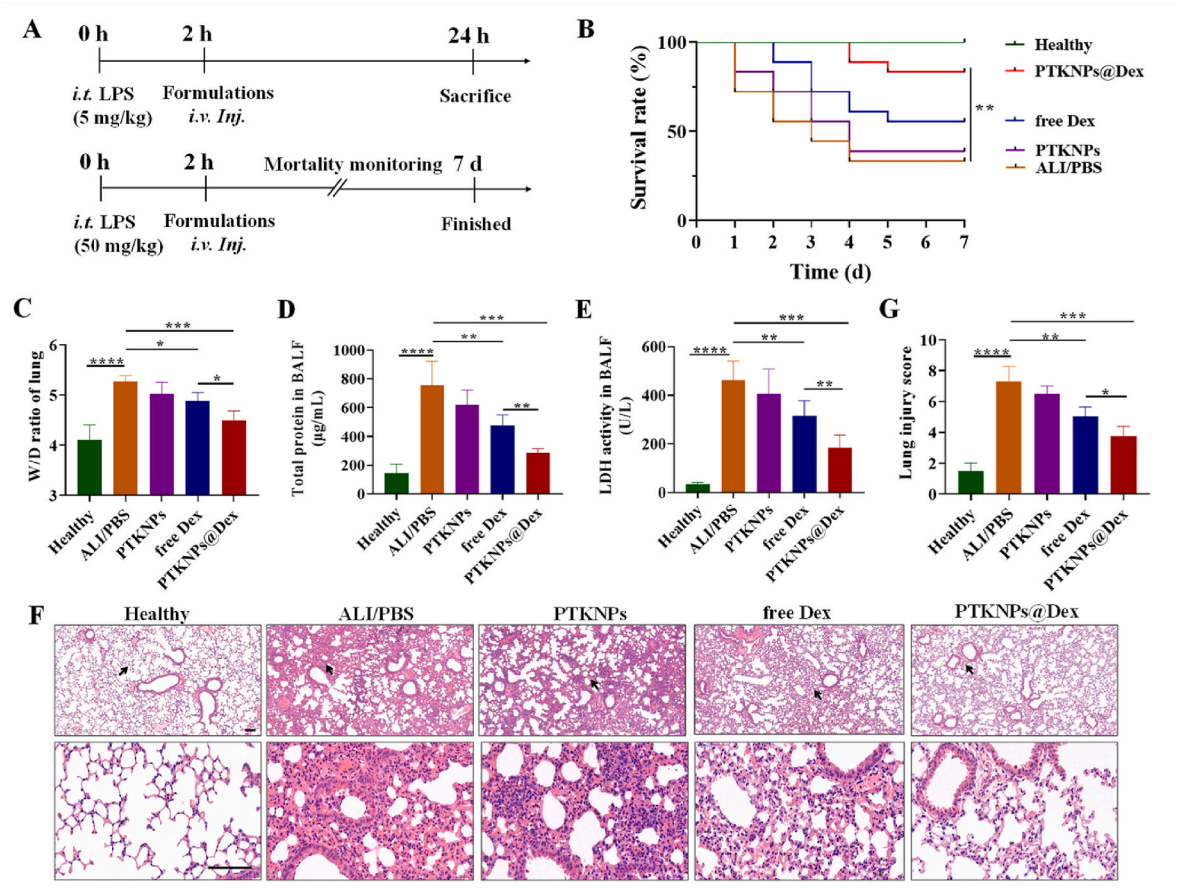

Fig. 3. Lung injury in LPS-induced ALI mice was alleviated by PTKNPs@Dex. (A) Experimental schedule of the ALI study *in vivo*. C57BL/6 mice were intratracheally injected with LPS to establish the ALI model. Two hours later, mice were received intravenous injection of different formulations. For the therapeutic analysis, the mice were sacrificed in 24 h after LPS (5 mg/kg) administration (upper panel), or observed every 24 h up to 7 d after LPS (50 mg/kg) administration to monitor the mortality (lower panel). (B) Mice survival rate. n = 12–18 mice/group. (C) Lung W/D ratio by various treatments. Levels of (D) total protein and (E) LDH in the BALF. n = 5 mice/group. (F) Representative H&E staining of lung tissues. The lower panel shows magnified images at the positions pointed out by the arrows on the upper panel. Scale bars are 100 μm and 50 μm for the overview and magnified images, respectively. (G) Histogram of lung injury scores. n = 3–5 mice/group. *p < 0.05, **p < 0.01, ***p < 0.001, and ****p < 0.0001.

such as liver and spleen at 96 h, whereas they did not show detectable toxicity judging from the normal physiological structure and cell morphology (Fig. S8) and had no signs of tissue damage or disturbances.

3.5. Therapeutic effect of NPs in ALI mice

Next, the NPs were tested for their efficacy on ALI in mice. Two hours after the LPS (5 mg/kg) challenge in the lungs of mice, the PBS, PTKNPs, free Dex (4 mg/kg) or PTKNPs@Dex (equal to 4 mg/kg of Dex) were *i.v.* administered (Fig. 3A). All of the mice were euthanized 22 h after *i.v.* injection to collect lung tissues and BALF (Fig. 3A, upper panel). Meanwhile, the survival rate was monitored every 24 h until 7 d after 10 folds of LPS was administered (Fig. 3A, lower panel). It was found that over 25% mice with ALI died within 24 h when they were treated with PBS (Fig. 3B). The PTKNPs alone had a slight better effect. Administration of free Dex could better prolong the survival time of mice and increase the survival rate. By a sharp contrast, the survival rate achieved 83.3% after treatment with the PTKNPs@Dex.

The characteristic of ALI is the influx of protein-rich edema fluid into the air spaces as a result of increased permeability of capillary endothelial-alveolar epithelial barrier [6]. The lung W/D ratio is a typical index of the pulmonary edema. Fig. 3C shows that the model group treated with PBS had a highest W/D ratio, showing a significant pulmonary edema. The PTKNPs-treated group showed an inhibition of edema to a certain degree. By contrast, the administration with free Dex and PTKNPs@Dex significantly reduced the W/D ratio, with the latter being smallest.

The analyses of total protein concentrations and LDH activity in BALF (Fig. 3D and E) further found the lowest edema fluid content and degree of injury in the PTKNPs@Dex group compared with all other groups, revealing the therapeutic efficiency that is consistent with the H&E staining (Fig. 3F). The ALI mice treated with PBS displayed severest inflammatory cells infiltration and alveolar hemorrhage, whereas the administration of PTKNPs@Dex could alleviate these histological injuries significantly, as demonstrated by the smallest lung injury score (Fig. 3G).

All these results reveal that the PTKNPs@Dex can effectively inhibit the influx of protein-rich edema fluid into alveolar, suppress the

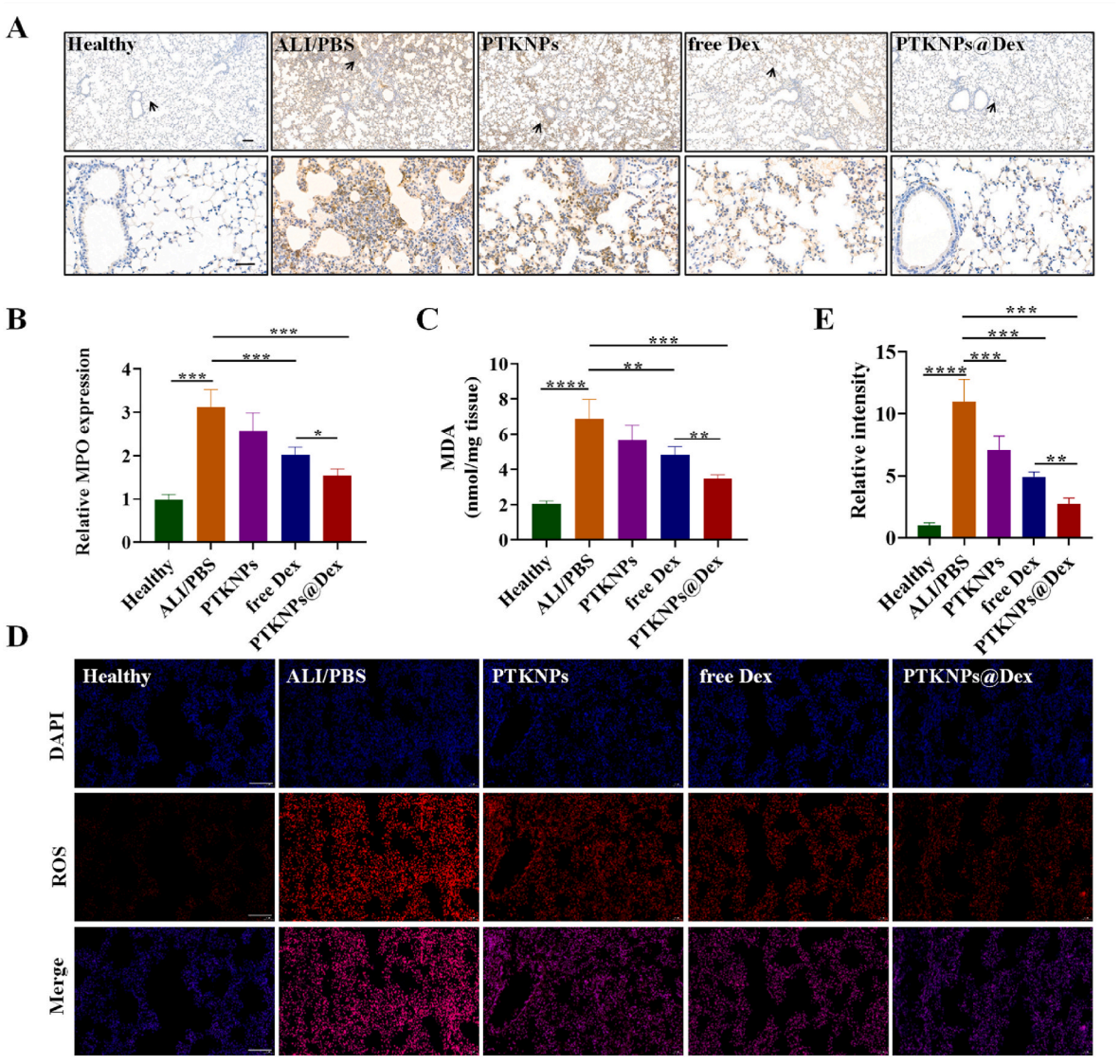

Fig. 4. PTKNPs@Dex suppressed oxidative damage and ROS level in LPS-induced ALI mice. (A) Representative images and (B) quantitative analysis of MPO in lung tissue after various treatments as indicated. The magnified images at the positions pointed out by the arrows are shown in the lower panel. Blue, nuclei; brown, MPO-positive cells. Scale bars are 100 μm and 40 μm for the overview and magnified images, respectively. n = 3–5 mice/group. (C) MDA level of lung tissue homogenates. n = 5 mice/group. (D) Representative images and (E) quantitative analysis of ROS production in lung tissue after being stained with DAPI (blue, nuclei) and DHE (red, ROS). Scale bar, 100 μm. n = 4 mice/group. *p < 0.05, **p < 0.01, ***p < 0.001, and ****p < 0.0001.

inflammatory cells infiltration, and reduce lung injury and mortality of ALI mice.

3.6. Antioxidant ability of NPs in vivo

During the progression of ALI, the over produced ROS can oxidize proteins, lipids and DNAs [32], contributing to the injury of alveolar epithelial cells and capillary endothelial cells [33]. Therefore, the degree of tissue oxidative damage is a key index to evaluate the antioxidant ability of NPs. MPO, a leukocyte enzyme released by activated neutrophils and monocytes, forms oxidative substances and free radicals to kill pathogens [34]. However, it also promotes oxidative damage of host tissues at the inflammatory sites. As shown in Fig. 4A and B, there was excessive MPO in the lung tissue after LPS stimulation, revealing the infiltration of neutrophils. However, the levels of MPO were reduced remarkably after the administration of free Dex and PTKNPs@Dex, which are consistent with the results of MPO level in BALF (Fig. S9). MDA is the product of lipid peroxidation, which can cause the cross-linking polymerization of proteins, nucleic acids and other biomacromolecules, and thus has cytotoxicity [35]. The level of MDA in the lung homogenate was also decreased markedly with the treatment of Dex and PTKNPs@Dex, as compared with the ALI model group (Fig. 4C). It has to mention that the PTKNPs@Dex was most effective in suppressing the production of MPO and MDA in the inflamed lung tissues. Fig. 4D and E shows that the PTKNPs alone could reduce the ROS level significantly, indicating the excellent ROS-scavenging ability of our NPs

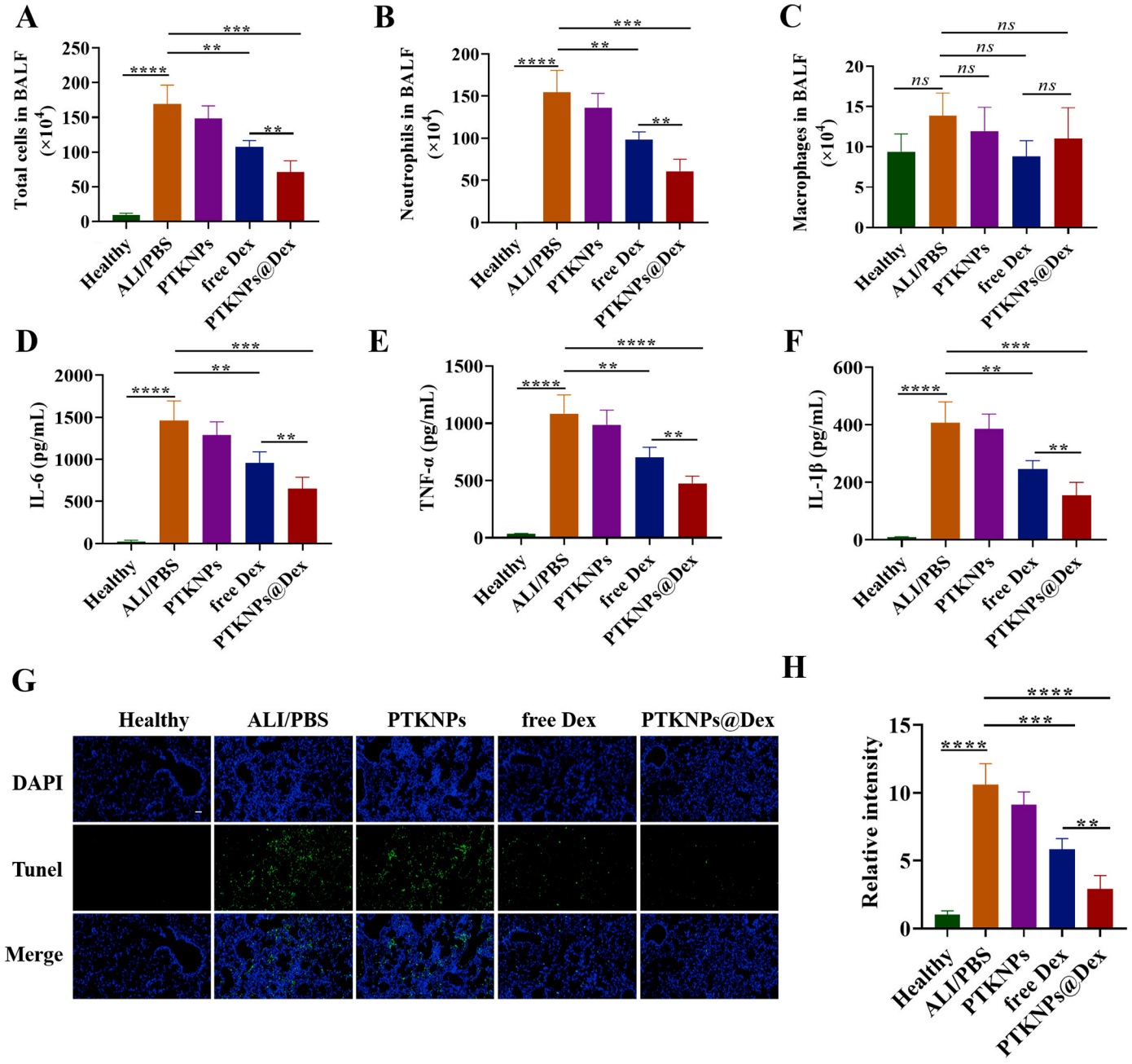

Fig. 5. PTKNPs@Dex reduced infiltration of inflammatory cells and suppressed inflammation in LPS-induced ALI mice. The number of (A) total cells, (B) neutrophils and (C) macrophages in BALF after various treatments as indicated. (D) IL-6, (E) TNF-α, and (F) IL-1β in BALF of different groups. n = 5 mice/group. (G) Representative images and (H) quantitative analysis of cell apoptosis in lung tissue after being stained with DAPI (blue, nuclei) and Tunel reaction solution (green, apoptotic cells). Scale bar, 50 μm. n = 3–5 mice/group. *p < 0.05, **p < 0.01, ***p < 0.001, and ****p < 0.0001; ns, no significant difference at p < 0.05.

in vivo. Again, the PTKNPs@Dex had the best ROS-suppression ability. Taken together, the PTKNPs@Dex have shown their synergetic effect on anti-oxidation, ROS-inhibition ability, and reduced neutrophils infiltration in ALI.

3.7. Anti-inflammation efficacy of NPs in vivo

The inflammatory cells play a crucial role in the development of ALI. The resident alveolar macrophages are first activated and turned to pro-inflammation phenotype M1, releasing various pro-inflammatory mediators that recruit neutrophils from the blood vessels to the air spaces [6]. Therefore, the number of inflammatory cells including macrophages and neutrophils were counted (Fig. 5A–C). The number of total cells was increased dramatically after LPS stimulation, and most of them were neutrophils, which are consistent with the fact that the ALI model induced by LPS is neutrophil-dependent [36]. Upon the treatment of PTKNPs@Dex, the number of total cells and neutrophils were decreased significantly as compared with other groups, demonstrating that the PTKNPs@Dex exhibited a satisfactory ability of inhibiting the neutrophils infiltration. Moreover, the levels of IL-6, TNF-α and IL-1β in BALF were further quantified by ELISA (Fig. 5D–F). Dex is a kind of glucocorticoids that inhibit the production of pro-inflammatory cytokines, exerting excellent anti-inflammation efficacy [37]. Consistently, the treatment of free Dex had an obvious inflammation inhibition effect in our animal experiment. The PTKNPs alone did not reduce the level of cytokines, whereas loading the Dex into PTKNPs had the best effect on the suppression of cytokine expression. Furthermore, the mRNA levels of pro-inflammatory M1 markers, including *Il-6, Tnf-α and Il-1β* in the lung tissue were analyzed by qPCR (Figs. S10A–C), showing the consistent results with the ELISA results. Besides, the PTKNPs@Dex could reduce the apoptosis of the lung tissue (Fig. 5G and H) to the best degree. Therefore, the PTKNPs@Dex exhibit significantly stronger anti-inflammation and anti-apoptosis efficacy in the ALI mice than either PTKNPs or free Dex treatment.

3.8. Mechanism of inflammatory suppression in vivo

As demonstrated by the above results, the PTKNPs@Dex exerted satisfactory anti-inflammatory, and anti-oxidative effects on ALI mice. Upon accumulation in the lung, the NPs were internalized by macrophages and neutrophils at the alveoli (Fig. S11), further released the loaded Dex. After being encapsulated into the PTKNPs, the Dex level in the lung was significantly enhanced compared with the free Dex group (Fig. S12), revealing the designed nanoplatform is an ideal carrier for the delivery of sufficient drugs to lung. To further understand the therapeutic effects of the PTKNPs@Dex at a molecular level, the transcriptional changes were quantified by RNA-Seq in the lung tissues. The differences in the mRNA levels of lung among the healthy control group,

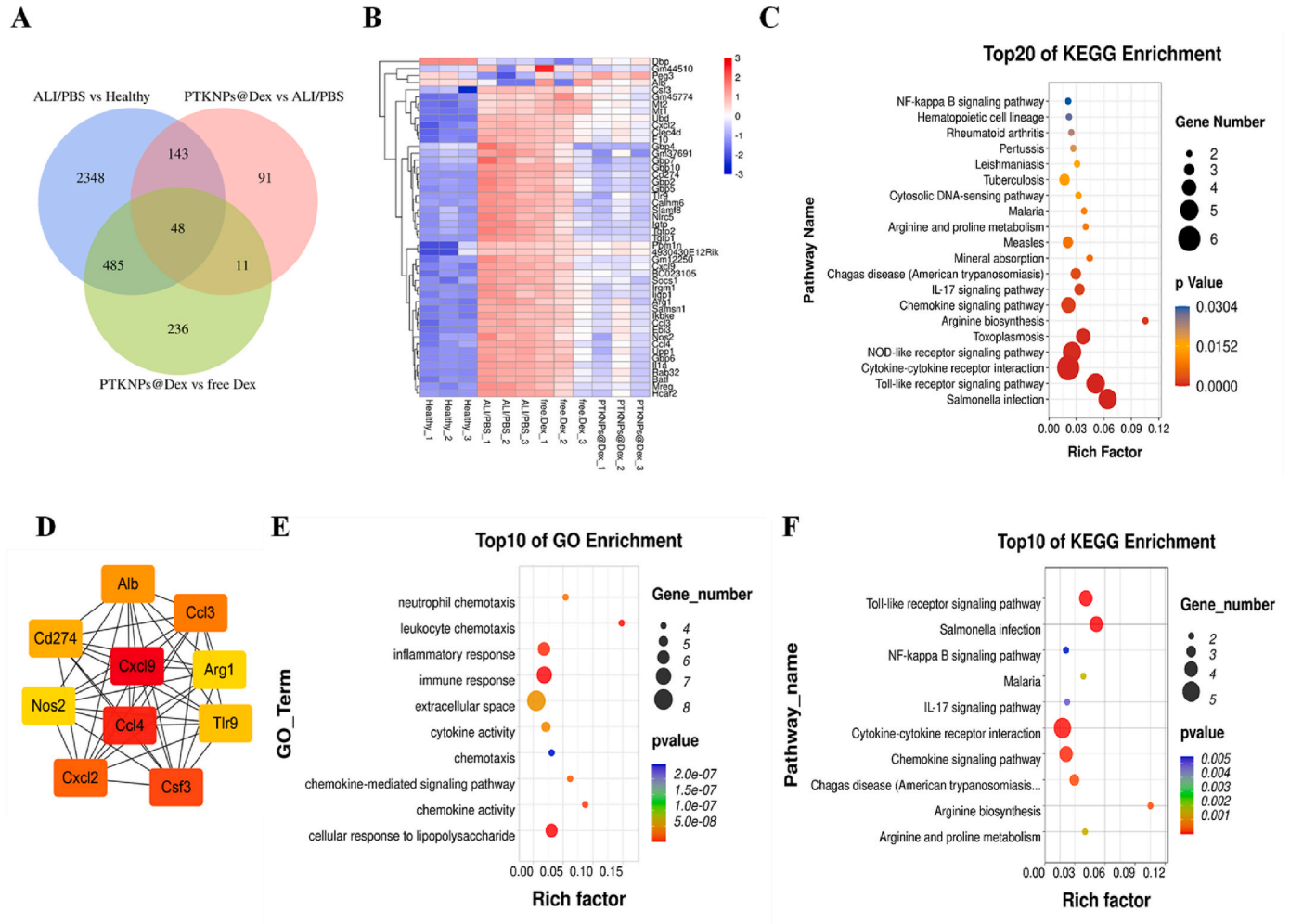

Fig. 6. Reduction of inflammation of LPS-induced ALI by PTKNPs@Dex identified from transcriptome levels. (A) Venn diagram showing the number of DEGs in intersection of the comparison groups in ALI/PBS (vs. Healthy), PTKNPs@Dex (vs. ALI/PBS) and PTKNPs@Dex (vs. free Dex) group. 48 DEGs were selected. (B) Heatmap of the 48 DEGs. (C) KEGG pathway analysis of the 48 DEGs. (D) PPI network analysis of the top 10 hub genes. Warm color nodes share higher connectivity degrees. (E) GO and (F) KEGG terms of the top 10 hub genes.

ALI model (ALI/PBS) group, PTKNPs group, free Dex group and PTKNPs@Dex group were thoroughly examined using a principal component analysis (PCA) and heatmap (Figs. S13A and B). Compared to the treatment of free Dex in the ALI mice, there were 280 upregulated and 500 downregulated DEGs in the PTKNPs@Dex group, which are shown in the volcano plots and heatmap (Figs. S14A and B). To deeply investigate the key DEGs regulated by the PTKNPs@Dex, the intersection of DEGs in the ALI/PBS (vs. Healthy), PTKNPs@Dex (vs. ALI/PBS) and PTKNPs@Dex (vs. free Dex) was further analyzed. The number of identified DEGs from different comparison groups is shown in Fig. S15A. The intersection of the above three datasets were selected, and 48 DEGs were clustered in a heatmap (Fig. 6A and B). To further investigate the potential pathways of the 48 DEGs, the KEGG was enriched in many pathways linked to the immune system and inflammatory pathways. The Toll-like receptor signaling pathway, cytokine-cytokine receptor interaction, and salmonella infection were the top 3 enriched pathways (Fig. 6C). To analyze the potential regulatory networks of these DEGs, the String database was used to predict the interactions among the 48 DEGs. The PPI network was visualized with Cytoscape software, including 41 nodes and 133 edges, of which 6 disconnected nodes were hidden. (Fig. S15B). To deeply investigate the key DEGs in the PPI network, we used the CytoHubba plugin-in of Cytoscape to select the top 10 hub genes with the highest degree of connectivity for further analysis, which ranked as *Cxcl9, Ccl4, Csf3, Cxcl2, Ccl3, Alb, Cd274, Tlr9, Arg1 and Nos2* (Fig. 6D). GO terms of these hub genes were specifically enriched in many immune response terms, including inflammatory response, chemokine and cytokine activity, leukocyte and neutrophil chemotaxis (Fig. 6E). The KEGG analysis of these hub genes was also enriched in many immune and inflammatory pathways, including Toll-like receptor signaling pathway, chemokine signaling pathway, NF-κB signaling pathway and IL-17 signaling pathway, which influence on the cytokine production, leukocyte recruitment, Th17 cell differentiation and inflammation (Fig. 6F). The WB results confirm that the PTKNPs@Dex decreased LPS-induced expression of IL-17A and phosphorylation of NF-κB *in vitro* and *in vivo* (Figs. S16A and B), which are the key proteins of IL-17 and NF-κB signaling pathway, respectively. Consistent with the RNA-Seq data, the expression of hub genes including *Cxcl9, Ccl4, Csf3, Cxcl2, Ccl3 and Nos2* in the lung tissue was validated by qPCR (Figs. S17A–F). These results indicate that the PTKNPs@Dex mainly modulate the immune and inflammatory-related pathways, leading to decreased nitric oxide synthesis, chemokine and cytokine production, and leukocyte recruitment, and thus contributing to less inflammation and tissue injury.

3.9. Effects of NPs on systemic inflammation and oxidative stress

During the onset and development of ALI/ARDS, systemic inflammation and oxidative stress are also serious [38]. As shown in Figs. S18A and B, the PTKNPs@Dex reduced the levels of IL-6 and TNF-α in serum significantly, suggesting that the designed NPs not only alleviate lung inflammation, but also inhibit the systemic inflammation. Moreover, with the treatment of PTKNPs, the level of MDA in blood was decreased significantly (Fig. S18C), which further confirms the outstanding anti-oxidative capacity of PTKNPs. However, there was only a slight decrease of MDA in lung tissue (Fig. 4C), likely because of the higher concentration of PTKNPs at blood than lung. Furthermore, the combination of PTKNPs and Dex resulted in the lowest MDA concentration. All these results reveal that the PTKNPs@Dex have a positive effect on suppressing systemic inflammation and oxidative stress, providing a promising candidate in clinical application in the future.

In summary, the PTKNPs@Dex composed of ROS-responsive thioketal polymers have shown a satisfactory therapeutic effect on ALI, whose inflammatory regulation ability is much more effective than that of non-ROS responsive DDS [39]. The ROS eliminating capacity is superior to other reported ROS-responsive DDS due to the massive thioketal bonds in the polymer main chains [40]. The NPs are not only the carriers to deliver drugs to the inflamed lung, but also ROS-scavenging agent to eliminate large amount of ROS first, and then release the drugs under the trigger of high level of ROS in the ALI, reducing the tissue oxidative damage. In addition, the NPs can effectively modulate the immune and inflammation-linked pathways, inhibiting inflammation at a molecular level. Nonetheless, the administration pathway and targeting ability of the NPs system can be still improved by conjugating inflammation or lung-targeting moieties and grafting sheath molecules that have been extensively explored previously [40].

4. Conclusions

The PTKNPs@Dex nanoplatform developed in this study showed a great potential as an inflammatory regulation therapy in LPS-induced ALI mice. Upon exposure to ROS, the NPs were degraded to consume ROS and release the anti-inflammatory drug (Dex) rapidly, showing excellent ROS-scavenging ability and inflammatory suppression *in vitro*. With the synergetic anti-oxidative and anti-inflammatory effects, the PTKNPs@Dex exerted greater efficacy than either free Dex or PTKNPs alone in the ALI treatment, significantly improving the survival rate of mice, and attenuating lung injury, inflammatory infiltration, oxidative tissue damage and pro-inflammatory factors via modulating immune and inflammation-linked pathways. With the strong biological functions, good biocompatibility, low toxicity and ease of preparation, the ROS-responsive and anti-inflammation nanoplatform is highly favorable in addressing the inflammation-related diseases besides the ALI shown in this study.

Data availability statement

The raw/processed data can be requested from the authors.

CRediT authorship contribution statement

Zihe Zhai: Investigation, Methodology, Writing – original draft. **Wei Ouyang:** Investigation, Methodology, Writing – original draft. **Yuejun Yao:** Formal analysis. **Yuqi Zhang:** Methodology. **Haolan Zhang:** Formal analysis. **Feng Xu:** Conceptualization, Project administration. **Changyou Gao:** Conceptualization, Project administration, Writing – review & editing.

Declaration of competing interest

There are no conflicts to declare.

Acknowledgements

This study is financially supported by the Natural Science Foundation of Zhejiang Province (LD21E030001), National Natural Science Foundation of China (51873188, 81770008), and the Fundamental Research Funds for the Central Universities of China (2020XZZX004-01).

Appendix A. Supplementary data

Supplementary data to this article can be found online at https://doi.org/10.1016/j.bioactmat.2022.01.047.

References

[1] R. Medzhitov, Origin and physiological roles of inflammation, Nature 454 (7203) (2008) 428–435.
[2] K.J. Tracey, The inflammatory reflex, Nature 420 (6917) (2002) 853–859.
[3] C. Huang, Y. Wang, X. Li, L. Ren, J. Zhao, Y. Hu, L. Zhang, G. Fan, J. Xu, X. Gu, Z. Cheng, T. Yu, J. Xia, Y. Wei, W. Wu, X. Xie, W. Yin, H. Li, M. Liu, Y. Xiao, H. Gao, L. Guo, J. Xie, G. Wang, R. Jiang, Z. Gao, Q. Jin, J. Wang, B. Cao, Clinical features

of patients infected with 2019 novel coronavirus in wuhan, China, Lancet 395 (10223) (2020) 497–506.
[4] D. Chu, J. Gao, Z. Wang, Neutrophil-mediated delivery of therapeutic nanoparticles across blood vessel barrier for treatment of inflammation and infection, ACS Nano 9 (12) (2015) 11800–11811.
[5] Z. Wang, J. Li, J. Cho, A.B. Malik, Prevention of vascular inflammation by nanoparticle targeting of adherent neutrophils, Nat. Nanotechnol. 9 (3) (2014) 204–210.
[6] B.T. Thompson, R.C. Chambers, K.D. Liu, Acute respiratory distress syndrome, N. Engl. J. Med. 377 (6) (2017) 562–572.
[7] M.A. Matthay, L.B. Ware, G.A. Zimmerman, The acute respiratory distress syndrome, J. Clin. Invest. 122 (8) (2012) 2731–2740.
[8] M.A. Matthay, R.L. Zemans, The acute respiratory distress syndrome: pathogenesis and treatment, Annu. Rev. Pathol. 6 (1) (2011) 147–163.
[9] A.B. Cook, P. Decuzzi, Harnessing endogenous stimuli for responsive materials in theranostics, ACS Nano 15 (2) (2021) 2068–2098.
[10] Z. Zhai, W. Zhang, N. Ding, X. Lin, C. Gao, Protrusion of nanospikes on cholesterol-containing microgels by reduction-responsive self-assembly in cell milieu and its influence on cell functions, Mater. Chem. Front. 3 (2) (2019) 233–241.
[11] Y. Wang, M.S. Shim, N.S. Levinson, H.-W. Sung, Y. Xia, Stimuli-responsive materials for controlled release of theranostic agents, Adv. Funct. Mater. 24 (27) (2014) 4206–4220.
[12] Y.J. Yao, H.L. Zhang, Z.Y. Wang, J. Ding, S.Q. Wang, B.Q. Huang, S.F. Ke, C.Y. Gao, Reactive oxygen species (ros)-responsive biomaterials mediate tissue microenvironments and tissue regeneration, J. Mater. Chem. B 7 (33) (2019) 5019–5037.
[13] Y. Wang, Q. Yuan, W. Feng, W. Pu, J. Ding, H. Zhang, X. Li, B. Yang, Q. Dai, L. Cheng, J. Wang, F. Sun, D. Zhang, Targeted delivery of antibiotics to the infected pulmonary tissues using ros-responsive nanoparticles, J. Nanobiotechnol. 17 (1) (2019) 103.
[14] B. Ma, H. Xu, W. Zhuang, Y. Wang, G. Li, Y. Wang, Reactive oxygen species responsive theranostic nanoplatform for two-photon aggregation-induced emission imaging and therapy of acute and chronic inflammation, ACS Nano 14 (5) (2020) 5862–5873.
[15] Y. Zhang, H. Zhang, Z. Mao, C. Gao, Ros-responsive nanoparticles for suppressing the cytotoxicity and immunogenicity caused by pm2.5 particulates, Biomacromolecules 20 (4) (2019) 1777–1788.
[16] C. Zhao, J. Chen, J. Ye, Z. Li, L. Su, J. Wang, Y. Zhang, J. Chen, H. Yang, J. Shi, J. Song, Structural transformative antioxidants for dual-responsive anti-inflammatory delivery and photoacoustic inflammation imaging, Angew. Chem. Int. Ed. 60 (26) (2021) 14458–14466.
[17] D.S. Wilson, G. Dalmasso, L. Wang, S.V. Sitaraman, D. Merlin, N. Murthy, Orally delivered thioketal nanoparticles loaded with tnf-alpha-sirna target inflammation and inhibit gene expression in the intestines, Nat. Mater. 9 (11) (2010) 923–928.
[18] H. Zhang, H. Xiong, W. Ahmed, Y. Yao, S. Wang, C. Fan, C. Gao, Reactive oxygen species-responsive and scavenging polyurethane nanoparticles for treatment of osteoarthritis in vivo, Chem. Eng. J. 409 (2021), 128147.
[19] Z. Tang, C. He, H. Tian, J. Ding, B.S. Hsiao, B. Chu, X. Chen, Polymeric nanostructured materials for biomedical applications, Prog. Polym. Sci. 60 (2016) 86–128.
[20] J. Ding, Y.J. Yao, J.W. Li, Y.Y. Duan, J.R. Nakkala, X. Feng, W.B. Cao, Y.C. Wang, L. J. Hong, L.Y. Shen, Z.W. Mao, Y. Zhu, C.Y. Gao, A reactive oxygen species scavenging and o-2 generating injectable hydrogel for myocardial infarction treatment in vivo, Small 16 (48) (2020), 2005038.
[21] W. Ouyang, H. Zhou, C. Liu, S. Wang, Y. Han, J. Xia, F. Xu, 25-hydroxycholesterol protects against acute lung injury via targeting md-2, J. Cell Mol. Med. 22 (11) (2018) 5494–5503.
[22] W. Ouyang, M. Cen, L. Yang, W. Zhang, J. Xia, F. Xu, Nmi facilitates influenza a virus infection by promoting degradation of irf7 through trim 21, Am. J. Respir. Cell Mol. Biol. 65 (1) (2021) 30–40.
[23] F. El-Mohtadi, R. d'Arcy, N. Tirelli, Oxidation-responsive materials: biological rationale, state of the art, multiple responsiveness, and open issues, Macromol. Rapid Commun. 40 (1) (2019), 1800699.
[24] J. Herzberger, K. Fischer, D. Leibig, M. Bros, R. Thiermann, H. Frey, Oxidation-responsive and "clickable" poly(ethylene glycol) via copolymerization of 2-(methylthio)ethyl glycidyl ether, J. Am. Chem. Soc. 138 (29) (2016) 9212–9223.
[25] R. d'Arcy, A. Siani, E. Lallana, N. Tirelli, Influence of primary structure on responsiveness. Oxidative, thermal, and thermo-oxidative responses in polysulfides, Macromolecules 48 (22) (2015) 8108–8120.
[26] D. Jeanmaire, J. Laliturai, A. Almalik, P. Carampin, R. d'Arcy, E. Lallana, R. Evans, R.E.P. Winpenny, N. Tirelli, Chemical specificity in redox-responsive materials: the diverse effects of different reactive oxygen species (ros) on polysulfide nanoparticles, Polym. Chem. 5 (4) (2014) 1393–1404.
[27] N.R. Aggarwal, L.S. King, F.R. D'Alessio, Diverse macrophage populations mediate acute lung inflammation and resolution, Am. J. Physiol. Lung Cell Mol. Physiol. 306 (8) (2014) L709–L725.
[28] B. Wang, Y. Zhang, Z. Mao, C. Gao, Cellular uptake of covalent poly(allylamine hydrochloride) microcapsules and its influences on cell functions, Macromol. Biosci. 12 (11) (2012) 1534–1545.
[29] Q. Xu, C. He, C. Xiao, X. Chen, Reactive oxygen species (ros) responsive polymers for biomedical applications, Macromol. Biosci. 16 (5) (2016) 635–646.
[30] Q. Qiao, X. Liu, T. Yang, K. Cui, L. Kong, C. Yang, Z. Zhang, Nanomedicine for acute respiratory distress syndrome: the latest application, targeting strategy, and rational design, Acta Pharm. Sin. B 11 (10) (2021) 3060–3091.
[31] S. Haque, C.W. Pouton, M.P. McIntosh, D.B. Ascher, D.W. Keizer, M.R. Whittaker, L.M. Kaminskas, The impact of size and charge on the pulmonary pharmacokinetics and immunological response of the lungs to plga nanoparticles after intratracheal administration to rats, Nanomed. Nanotechnol. Biol. Med. 30 (2020), 102291.
[32] G. Perry, A.K. Raina, A. Nunomura, T. Wataya, L.M. Sayre, M.A. Smith, How important is oxidative damage? Lessons from alzheimer's disease, Free Radical Biol. Med. 28 (5) (2000) 831–834.
[33] D. Mehta, A.B. Malik, Signaling mechanisms regulating endothelial permeability, Physiol. Rev. 86 (1) (2006) 279–367.
[34] R. Zhang, M.-L. Brennan, X. Fu, R.J. Aviles, G.L. Pearce, M.S. Penn, E.J. Topol, D. L. Sprecher, S.L. Hazen, Association between myeloperoxidase levels and risk of coronary artery disease, JAMA 286 (17) (2001) 2136–2142.
[35] K. Jomova, M. Valko, Advances in metal-induced oxidative stress and human disease, Toxicology 283 (2–3) (2011) 65–87.
[36] E. Kolaczkowska, P. Kubes, Neutrophil recruitment and function in health and inflammation, Nat. Rev. Immunol. 13 (3) (2013) 159–175.
[37] N. Auphan, J.A. DiDonato, C. Rosette, A. Helmberg, M. Karin, Immunosuppression by glucocorticoids: inhibition of nf-κb activity through induction of iκb synthesis, Science 270 (5234) (1995) 286–290.
[38] G. Matute-Bello, C.W. Frevert, T.R. Martin, Animal models of acute lung injury, Am. J. Physiol. Lung Cell Mol. Physiol. 295 (3) (2008) L379–L399.
[39] Q. Ma, Q. Fan, J. Xu, J. Bai, X. Han, Z. Dong, X. Zhou, Z. Liu, Z. Gu, C. Wang, Calming cytokine storm in pneumonia by targeted delivery of tpca-1 using platelet-derived extracellular vesicles, Matter 3 (1) (2020) 287–301.
[40] C.Y. Zhang, W. Lin, J. Gao, X. Shi, M. Davaritouchaee, A.E. Nielsen, R.J. Mancini, Z. Wang, Ph-responsive nanoparticles targeted to lungs for improved therapy of acute lung inflammation/injury, ACS Appl. Mater. Interfaces 11 (18) (2019) 16380–16390.